




# Efficient incorporation and template-dependent polymerase inhibition are major determinants for the broad-spectrum antiviral activity of remdesivir

Received for publication, October 14, 2021, and in revised form, December 17, 2021. Published, Papers in Press, December 23, 2021,

<https://doi.org/10.1016/j.jbc.2021.101529>

Calvin J. Gordon<sup>1,‡</sup>, Hery W. Lee<sup>1,‡</sup> , Egor P. Tchesnokov<sup>1,‡</sup>, Jason K. Perry<sup>2</sup>, Joy Y. Feng<sup>2</sup>, John P. Bilello<sup>2</sup> , Danielle P. Porter<sup>2</sup>, and Matthias Götte<sup>1,\*</sup>

From the <sup>1</sup>Department of Medical Microbiology and Immunology, University of Alberta, Edmonton, Alberta, Canada; <sup>2</sup>Gilead Sciences, Inc, Foster City, California, USA

Edited by Craig Cameron

Remdesivir (RDV) is a direct-acting antiviral agent that is approved in several countries for the treatment of coronavirus disease 2019 caused by the severe acute respiratory syndrome coronavirus 2. RDV exhibits broad-spectrum antiviral activity against positive-sense RNA viruses, for example, severe acute respiratory syndrome coronavirus and hepatitis C virus, and nonsegmented negative-sense RNA viruses, for example, Nipah virus, whereas segmented negative-sense RNA viruses such as influenza virus or Crimean-Congo hemorrhagic fever virus are not sensitive to the drug. The reasons for this apparent efficacy pattern are unknown. Here, we expressed and purified representative RNA-dependent RNA polymerases and studied three biochemical parameters that have been associated with the inhibitory effects of RDV-triphosphate (TP): (i) selective incorporation of the nucleotide substrate RDV-TP, (ii) the effect of the incorporated RDV-monophosphate (MP) on primer extension, and (iii) the effect of RDV-MP in the template during incorporation of the complementary UTP. We found a strong correlation between antiviral effects and efficient incorporation of RDV-TP. Inhibition in primer extension reactions was heterogeneous and usually inefficient at higher NTP concentrations. In contrast, template-dependent inhibition of UTP incorporation opposite the embedded RDV-MP was seen with all polymerases. Molecular modeling suggests a steric conflict between the 1'-cyano group of the inhibitor and residues of the structurally conserved RNA-dependent RNA polymerase motif F. We conclude that future efforts in the development of nucleotide analogs with a broader spectrum of antiviral activities should focus on improving rates of incorporation while capitalizing on the inhibitory effects of a bulky 1'-modification.

The coronavirus disease 2019 (COVID-19) caused by severe acute respiratory syndrome coronavirus 2 (SARS-CoV-2) revealed the importance of broad-spectrum antivirals as the first line of defense in a pandemic (1, 2). Vaccines that

effectively protect against severe COVID-19 were developed in less than a year after the World Health Organization declared a pandemic in March 2020 (3–6). Antibody therapies, directed specifically against SARS-CoV-2, were also developed in a relatively short time and the first antiviral drug approved for the treatment of COVID-19 was the nucleotide analog prodrug remdesivir (RDV) (7). Its broad spectrum of antiviral activity was described in earlier preclinical studies (8–17). RDV is a 1'-cyano modified C-adenosine monophosphate prodrug that targets the RNA-dependent RNA polymerase (RdRp) of a diverse panel of RNA viruses, including coronaviruses (8, 13, 18–20). In 2019, before the COVID-19 pandemic, RDV was tested in a randomized clinical phase 3 trial for the treatment of Ebola virus disease (21). Although the clinical efficacy of RDV against Ebola virus disease is inferior to two antibody therapies, its human safety data became available and this enabled RDV compassionate use in January 2020 to treat COVID-19 patients (22).

Clinical studies of RDV for the treatment of COVID-19 have shown a shortened time to recovery with an unclear effect on mortality (23, 24). RDV is intravenously administered and is therefore limited to patients under supervised medical care. In general, oral antiviral drugs would allow earlier initiation of treatment in a broader patient population, which may reduce the risk of progression to more severe disease outcomes, not only in the context of infection with coronaviruses but potentially for the treatment of other viral infections. The development of oral broad-spectrum antiviral drugs is therefore critical to public health and pandemic preparedness. Successful efforts in this field require a better understanding of biochemical mechanisms that translate to antiviral activity. RDV shows antiviral activity against human positive-sense RNA viruses including the members of *Coronaviridae* (SARS-CoV, Middle Eastern respiratory syndrome, MERS-CoV, and SARS-CoV-2) (8, 19) and the *Flaviviridae* (hepatitis C virus, HCV) (20), as well as nonsegmented negative-sense RNA viruses including members of the *Filoviridae* (Zaire Ebola virus [Ebola virus, EBOV]), *Pneumoviridae* (respiratory syncytial virus [RSV]), and *Paramyxoviridae* (Nipah virus [NiV]) (13). However, antiviral activity against segmented negative-

<sup>‡</sup> These authors contributed equally to this work.

\* For correspondence: Matthias Götte, [gotte@ualberta.ca](mailto:gotte@ualberta.ca).

## Broad-spectrum activity of remdesivir

sense RNA viruses is less pronounced or not significant, as shown with members of the *Arenaviridae* (Lassa virus [LASV]), the *Orthomyxoviridae* (influenza virus), and *Nairoviridae* (Crimean-Congo hemorrhagic fever virus [CCHFV]) (13, 20).

Here, we expressed and purified representative RdRp enzymes or complexes associated with these different families of RNA viruses and studied biochemical mechanisms of RDV-mediated inhibition of RNA synthesis to better understand the molecular requirements for antiviral effects. Previous studies with purified SARS-CoV, MERS-CoV, and SARS-CoV-2 RdRp complexes have shown that the triphosphate (TP) form of RDV (RDV-TP) is 2 to 3 times more efficiently incorporated than its natural counterpart ATP (25–28). Inhibition is not seen immediately downstream of the site of RDV-monophosphate (MP) incorporation “i”, it is rather seen at position “i + 3” after the addition of three more nucleotides (25, 26). This pattern is consistent with the definition of “delayed chain-terminators” that inhibit nucleotide incorporation events distant from the site of incorporation (29, 30). Per definition, “termination” is not necessarily absolute and may be overcome with longer reaction times or increasing NTP concentrations (11, 16, 29–35). For Ebola RdRp, it has been shown that delayed chain-termination with RDV-TP is in fact absolute at position i + 5 (16). For SARS-CoV-2 RdRp, it has been demonstrated that higher NTP concentrations can overcome inhibition at “i + 3” (26, 27, 36–39). Others have therefore used a different terminology and refer to “delayed translocation” (39), “delayed chain extension” (39), “delayed stalling” (36), “delayed intervention” (40), or enzyme “pausing” (27, 37, 40, 41). “Pausing” has also been observed on long templates that better mimic the RNA genome (37). Most importantly, continuation of RNA synthesis would yield newly synthesized RNA strands with embedded RDV-MP residues, and these RNAs will later serve as templates. We have recently

shown that the incorporation of UTP opposite the complementary RDV-MP provides a second opportunity for inhibition (42). We now demonstrate that this template-dependent inhibition of RNA synthesis is observed across a diverse panel of viral polymerases. However, efficient incorporation of RDV-TP is a prerequisite for downstream inhibition of RNA synthesis and its translation into antiviral activity.

## Results

### Selective incorporation of RDV-TP

To address the differences seen in the antiviral activity of RDV against a diverse spectrum of virus families, we compared the efficiency and pattern of inhibition of recombinant RdRp enzymes or enzyme complexes representing members of relevant families of viruses and for which antiviral activity data were available (Table 1). Partial biochemical data were available for SARS-CoV, MERS-CoV, SARS-CoV-2, EBOV, and RSV RdRp complexes. Here, we included polymerases from HCV and NiV that are also sensitive to RDV, LASV that is less sensitive to RDV, and influenza B (FluB) and CCHFV that are not sensitive to RDV in antiviral assays. RNA synthesis was monitored with short primer/templates mimicking random elongation complexes, as previously described (16, 25, 26, 42, 43). We first determined the steady-state kinetic parameters for RDV-TP incorporation for each RdRp and normalized the values to the rates of incorporation of ATP. The enzyme concentration is the same in both cases and therefore cancels out during the normalization. The ratio of efficiency of single incorporations of ATP over RDV-TP defines the selectivity, which is a unitless parameter that facilitates comparisons between enzymes. Selectivity is less than 1, if incorporation of the analog is more efficient than incorporation of its natural counterpart.

Previous data have shown that RdRp complexes of coronaviruses SARS-CoV, MERS-CoV, and SARS-CoV-2 produce

**Table 1**  
Selective incorporation of RDV-TP and antiviral activity against selected RNA viruses

Sense	Family	Virus	Incorporation in biochemical assays		Antiviral activity in cell culture	
			ATP/RDV-TP		GS-441524 <sup>b</sup>	RDV <sup>b</sup>
			Selectivity <sup>a</sup>		EC <sub>50</sub>	EC <sub>50</sub>
Positive ssRNA	<i>Coronaviridae</i>	SARS-CoV	0.32 <sup>c</sup>		0.18 <sup>d</sup>	0.069 <sup>d</sup>
		SARS-CoV-2	0.28 <sup>c</sup>		0.28–1.65 <sup>e</sup>	0.47–1.09 <sup>e</sup>
Nonsegmented negative ssRNA	<i>Flaviviridae</i>	MERS-CoV	0.35 <sup>i</sup>		0.869 <sup>f</sup>	0.115 <sup>f</sup>
		HCV	0.93		0.86 <sup>d</sup>	0.074 <sup>d</sup>
	<i>Filoviridae</i>	EBOV	4.0 <sup>c</sup>		4.1 <sup>g</sup>	0.085 <sup>g</sup>
	<i>Pneumoviridae</i>	RSV	2.7 <sup>j</sup>		1.0–3.1 <sup>h</sup>	0.003–0.021 <sup>h</sup>
	<i>Paramyxoviridae</i>	NiV	1.6		0.63 <sup>h</sup>	0.021 <sup>h</sup>
Segmented negative ssRNA	<i>Arenaviridae</i>	LASV	20 <sup>c</sup>		0.49–2.2 <sup>h</sup>	0.029–0.047 <sup>h</sup>
	<i>Nairoviridae</i>	CCHFV	41		No inhibition <sup>h</sup>	4.5 <sup>h</sup>
	<i>Orthomyxoviridae</i>	FluB	68		No inhibition <sup>h</sup>	No inhibition <sup>h</sup>
		FluA			27.9 <sup>g</sup>	

<sup>a</sup> Selectivity of each viral RNA polymerase for RDV-TP is calculated as the ratio of the  $V_{max}/K_m$  values for ATP and RDV-TP, respectively. EC<sub>50</sub> values are given in  $\mu$ M.

<sup>b</sup> Reported antiviral effects of RDV measured in cell culture.

<sup>c</sup> Data from Gordon *et al.*, 2020 (26).

<sup>d</sup> Data from Agostini *et al.*, 2018 (8).

<sup>e</sup> Data from Pruijssers *et al.*, 2020 (19).

<sup>f</sup> Data from Xie *et al.*, 2020 (58).

<sup>g</sup> Data from Cho *et al.*, 2012 (20).

<sup>h</sup> Data from Lo *et al.*, 2017 (13).

<sup>i</sup> Data from Gordon *et al.*, 2020 (25).

<sup>j</sup> Data from Tchesnokov *et al.*, 2020 (16).

an RDV-TP selectivity value of less than 1 ( $\sim 0.3$ ) (Table 1). The selectivity value obtained in our previous studies on SARS-CoV-2 RdRp using a steady-state approach is comparable with the value obtained in pre-steady-state assays that used much higher concentrations of ATP and RDV-TP (26, 28). Effective inhibitory concentrations ( $EC_{50}$ ) measured in cell-based assays demonstrate potent antiviral activity of RDV across virus families.  $EC_{50}$  values for RDV or its parent nucleoside (GS-441524) are in the submicromolar range. Here, we demonstrate that HCV RdRp incorporates RDV-TP with a low selectivity value (0.93) (Tables 1 and S1), indicating that both RDV-TP and ATP are used with similar efficiency at the ATP and RDV-TP concentrations used in our study. The published  $EC_{50}$  values between  $\sim 0.08 \mu\text{M}$  for RDV and  $\sim 4 \mu\text{M}$  for GS-441524 are also indicative of efficient antiviral activity, although the prodrug has greater activity. A similar range of  $EC_{50}$  values is observed with RDV against the nonsegmented negative-sense RNA viruses EBOV (0.003–0.021  $\mu\text{M}$ ), RSV (0.021  $\mu\text{M}$ ), and NiV (0.029–0.047  $\mu\text{M}$ ). The selectivity values are between 1.6 and 4, which are slightly higher when compared with our measurements for polymerases from the positive-sense RNA viruses. Conversely, RDV does not show significant antiviral activity against segmented RNA viruses CCHFV and FluB, and the  $EC_{50}$  value for LASV is relatively high ( $\sim 4.5 \mu\text{M}$  for RDV). Corresponding  $EC_{50}$  values have not been reported for GS-441524. In each of these cases, we also measured high selectivity values for RDV-TP incorporation, which are 20, 41, and 68, for LASV, CCHFV, and FluB, respectively. Thus, the combined results revealed a correlation between antiviral activity as measured in cell-based assays and efficient rates of incorporation of RDV-TP as measured in enzymatic assays. However, the incorporation of a nucleotide analog does not necessarily translate into inhibition of RNA synthesis. The overarching remaining question is whether a uniform mechanism of action may help explain the broad spectrum of antiviral activities associated with RDV.

#### Inhibition of RNA synthesis catalyzed by HCV RdRp

Previous biochemical and structural studies with SARS-CoV-2 RdRp have shown that the incorporated RDV-MP at position “i” causes inhibition of nucleotide incorporation at position “i + 3” due to a steric clash between the 1'-cyano group and the hydroxyl group of the conserved Ser-861 (26, 27, 36, 39, 40, 42). We further demonstrated that a Ser-861-Gly mutation eliminated this blockage (42). A structural comparison of SARS-CoV-2 and HCV identified Gly-410 of the HCV RdRp as the residue corresponding to Ser-861 in SARS-CoV-2 RdRp (Fig. S1). A similar mechanism of inhibition is therefore not expected with HCV RdRp. For SARS-CoV-2, the extent of inhibition at position 9 or “i + 3” depends crucially on the concentration of the nucleotide substrate at position “i + 4”. Low NTP concentrations favor inhibition, whereas high NTP concentrations override inhibition due to enhanced enzyme translocation. To monitor inhibition caused by RDV-TP, we used RNA templates with single sites of incorporation for RDV-TP and gradually increased the concentrations of the next NTP substrates

(Fig. 1). The incorporation of RDV-TP by SARS-CoV-2 RdRp resulted in inhibition of nucleotide incorporation at position 9 (i + 3) (Fig. 1B). For HCV RdRp, subtle inhibition of RNA synthesis was observed at the point of incorporation (position 6 or i) and no inhibition at position 9 or “i + 3” (Fig. 1C). Inhibition at position “i” is however easily overcome with low concentrations of the following NTP substrates. 50% read-through beyond the point of inhibition required a 10-fold greater nucleotide concentration for SARS-CoV-2 to overcome the inhibition at i + 3 as compared to HCV (Fig. 1D).

To study whether repeated incorporations of RDV-TP could increase overall inhibition, we used a template with longer stretch of uridines (Fig. 2A). RNA synthesis by SARS-CoV-2 and HCV RdRp was monitored under competitive conditions in which we used a constant concentration of ATP and increasing concentrations of RDV-TP. RNA synthesis by SARS-CoV-2 RdRp was inhibited at ratios of RDV-TP over ATP as low as 0.1 and as high as 25 (Fig. 2B, left). An apparent rescue of RNA synthesis is seen at higher ratios of inhibitor over the natural nucleotide. This observation results from efficient RDV-TP incorporation by the SARS-CoV-2 RdRp that overrides inhibition; however, these high ratios of RDV-TP over ATP are unlikely relevant in a cellular environment. The possibility for multiple incorporations of RDV-TP by HCV RdRp did not show any significant RNA synthesis inhibition at the level of the full template-length product. However, as seen in Figure 1C (right), the inhibitory effect at the site of RDV incorporation is more pronounced with higher RDV concentrations because the concentrations of the ATP and NTPs for subsequent incorporations are kept constant and are therefore not sufficient to overcome the inhibitory effect (Fig. 2B, right). These results demonstrate that although SARS-CoV-2 and HCV RdRp both incorporate RDV-TP with high efficiency, significant inhibition of primer extension reactions at the level of the full template-length product is solely seen with SARS-CoV-2 RdRp. Although RDV-mediated inhibition of RNA synthesis three nucleotides downstream of an incorporated RDV-MP may therefore contribute to the observed antiviral effects in coronaviruses, the antiviral effect of RDV against HCV is likely based on a different mechanism.

#### Template-dependent inhibition of HCV RNA synthesis

High rates of incorporation of RDV-TP along with mechanisms that overcome inhibition provide conditions that allow the synthesis of full-length RNA copies. These copies are modified with multiple RDV-MP residues that could affect RNA synthesis when used as templates. For SARS-CoV-2 RdRp, the RDV-MP in the template causes inhibition of the incorporation of complementary UTP and the following NTP. A similar mechanism is also considered for HCV RdRp (Fig. 3). We used RNA templates with a single RDV-MP incorporated at position 11. Both SARS-CoV-2 and HCV RdRp show inhibition at position 10 before the site of UTP incorporation. Increasing UTP concentration diminishes inhibition in both cases. HCV RdRp also requires a lower concentration of UTP to overcome this obstacle. Inhibition of SARS-CoV-2 RdRp is also seen at the adjacent position that requires ATP

## Broad-spectrum activity of remdesivir

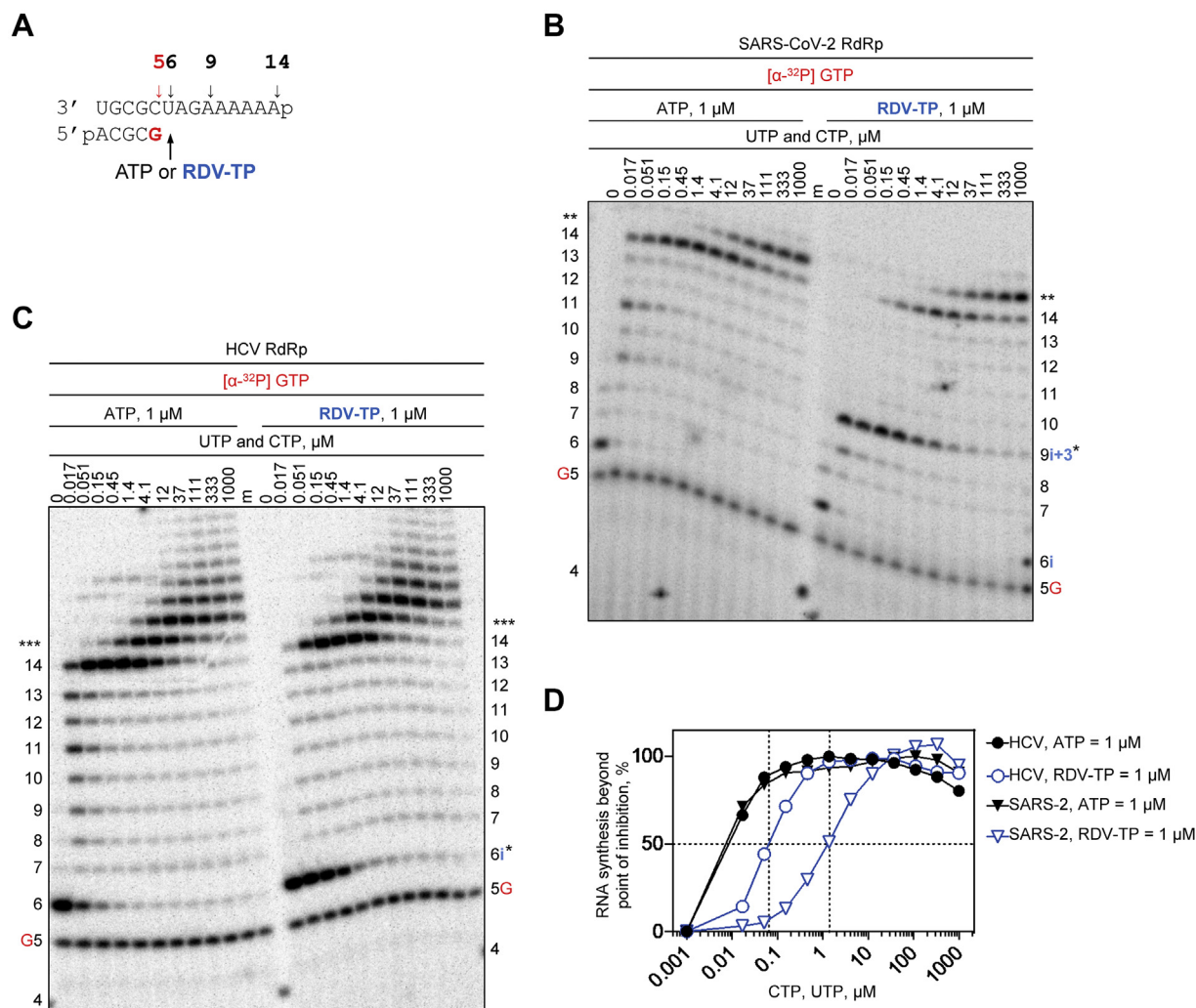


**Figure 1. SARS-CoV-2 or HCV RdRp-catalyzed RNA synthesis and inhibition patterns following a single incorporation of RDV-MP as a function of nucleotide concentration.** *A*, RNA primer/template supporting a single incorporation event of AMP or RDV-MP at position 5. *B*, migration pattern of the products of RNA synthesis catalyzed by SARS-CoV-2 RdRp. A 5'-<sup>32</sup>P-labeled 4-nt primer (4) serves as a size marker. The asterisk indicates the point at which RNA synthesis is inhibited (position 9 or "i + 3"). Two asterisks indicate slippage products that are likely sequence-dependent. *C*, reactions with HCV RdRp, inhibition of RNA synthesis occurs at the site of RDV-MP (position 6 or "i"). Three asterisks indicate increased slippage, likely sequence- and nucleotide-dependent. *D*, graphical representation of RNA synthesis beyond the point of RDV-TP induced inhibition for SARS-CoV-2 RdRp ("i + 3") and HCV RdRp ("i"). HCV, hepatitis C virus; MP, monophosphate; RdRp, RNA-dependent RNA polymerases; RDV, remdesivir; SARS-CoV-2, severe acute respiratory syndrome coronavirus 2; TP, triphosphate.

incorporation, whereas inhibition of HCV is confined to position 10. As a result of these two effects, overall inhibition of RNA synthesis is more pronounced for SARS-CoV-2 RdRp. Increasing both UTP and ATP concentrations yielded more full-length product, indicating that this obstacle is eventually overcome as well (Fig. S2). For both SARS-CoV-2 and HCV RdRp, template-dependent inhibition is more pronounced than the inhibitory effects in primer extension reactions.

### Embedded RDV-MP demonstrates a uniform mechanism of inhibition

It has previously been reported that RDV-TP causes "delayed chain-termination" in the context of NiV RdRp (11). NiV RdRp RNA synthesis was here monitored after a single RDV-TP or ATP incorporation in conjunction with increasing NTP concentrations (Fig. 4A). However, we were unable to

detect significant inhibitory effects under these conditions. Similar patterns of intermediate reaction products were seen after AMP and RDV-MP incorporation. In the absence of significant inhibition, the newly synthesized RNA strand will contain embedded RDV-MP residues. Using the same approach as above, RNA synthesis inhibition was again seen opposite RDV-MP at position 11 (Fig. 4B). Incorporation opposite templated RDV-MP and AMP, respectively, was evaluated with the increasing concentrations of UTP. Templated AMP allowed RNA synthesis to proceed to the full-length RNA at a UTP concentration as low as 4  $\mu$ M. In contrast, a UTP concentration up to 1000  $\mu$ M was not sufficient to support incorporation opposite RDV-MP, thus halting RNA synthesis at position 10 (Fig. 4B). Previous work with RSV and EBOV RdRp revealed the difficulties in identifying a template that enables the investigation of a single RDV-TP incorporation and generation of full template-length product

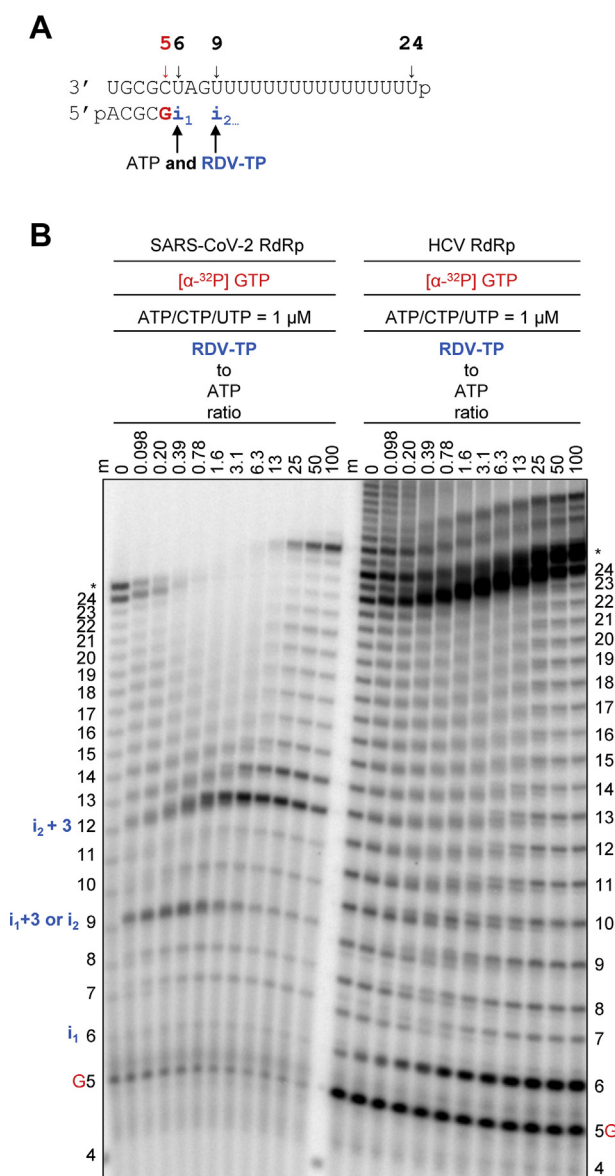


**Figure 2. SARS-CoV-2 or HCV RdRp-catalyzed RNA synthesis following multiple incorporations of RDV-MP as a function of RDV-TP concentration in the presence of a constant NTP concentration.** A, RNA primer/template supporting multiple incorporation events of ATP or RDV-TP. B, migration pattern of the products of RNA synthesis catalyzed by SARS-CoV-2 RdRp (left), first and second incorporation of RDV-TP occurs at position 6 ( $i_1$ ) and 9 ( $i_2$ ), respectively, with inhibition appearing at position 9 ( $i_1 + 3$ ) and 12 ( $i_2 + 3$ ). Migration pattern of HCV RdRp (right), minor product accumulation occurs at position 6, but inhibition of RNA synthesis resulting in full template-length product is not evident. The asterisk likely indicates reactions products due to slippage events. HCV, hepatitis C virus; MP, monophosphate; RdRp, RNA-dependent RNA polymerases; RDV, remdesivir; SARS-CoV-2, severe acute respiratory syndrome coronavirus 2; TP, triphosphate.

(16, 25). However, multiple incorporations of RDV-TP can cause “delayed chain-termination” with RSV and EBOV RdRp at position  $i + 5$  (16, 17). Here, we also examined RNA synthesis opposite the embedded RDV-MP at position 11 of the template (Fig. S3). RSV RdRp-catalyzed RNA synthesis could not proceed beyond the embedded RDV-MP even at the highest NTP concentrations, with most of the product accumulating at position 10 (Fig. S3B). The diminished processivity

of EBOV RdRp makes it difficult to accurately determine RNA synthesis and its inhibition beyond ten nucleotides (Fig. S3C).

Finally, we studied the inhibitory effects of RDV-TP or RDV-MP against RdRp enzymes from segmented negative-sense RNA viruses. We have previously demonstrated that RDV-TP is also a weak substrate for LASV RdRp, and its incorporation does not cause significant inhibition (26). Here, we demonstrate that the embedded RDV-MP in the template causes a complete stop of RNA synthesis (Fig. S3D). For FluB RdRp, the presence of RDV-TP also does not mediate significant inhibition of RNA synthesis (Fig. 5A). Minor differences in the degree of full-length product formed can likely be attributed to the inefficient incorporation of RDV-TP as compared to ATP. The templates containing AMP and RDV-MP, respectively, demonstrate again that the embedded RDV-MP causes RNA synthesis arrest at position 10 (Fig. 5B). A very similar pattern is seen with CCHFV RdRp (Fig. 6, A and B). No significant inhibition by RDV-TP in primer extensions and strong inhibition or even termination when RDV-MP is embedded in the template. However, inhibition translates to antiviral effects only if the rate of incorporation of RDV-TP is sufficiently high, which is unlikely the case for LASV, FluB, and CCHFV RdRp.

## Discussion

We compared the inhibitory effects of RDV-TP against a panel of viral RNA polymerases that represent diverse families of RNA viruses. The goal was to identify correlations between antiviral effects as previously measured in cell-based assays and the mechanism of inhibition.

Members of the positive-sense *Coronaviridae* (SARS-CoV-2) and *Flaviviridae* (HCV) families, as well as the nonsegmented negative-sense *Pneumoviridae* (RSV), *Filoviridae* (EBOV), and *Paramyxoviridae* (NiV) families are sensitive to RDV treatment, whereas members of the segmented negative-sense *Arenaviridae* (LASV), *Orthomyxoviridae* (FluB), and *Nairoviridae* (CCHFV) families are not sensitive to the drug (8, 13, 19, 20). We expressed the corresponding RdRp enzymes or enzyme complexes and studied: (i) selective incorporation of the nucleotide substrate RDV-TP, (ii) the effect of the incorporated RDV-MP on primer extensions, and (iii) the effect of the template-embedded RDV-MP on UTP incorporation.

Efficient selective incorporation of RDV-TP, calculated as the ratio of efficiency of incorporation of ATP over RDV-TP, is seen with SARS-CoV-2 (0.3), HCV (0.9), EBOV (4.0), NiV (1.6), and RSV enzymes (2.7). In contrast, much higher selectivity values for LASV (20), CCHFV (41), and FluB (68) enzymes suggest poor RDV-TP substrate usage. The ability of a nucleotide analog inhibitor to be incorporated by viral RdRp enzymes is largely dependent on variations in the residues that define the nucleotide-binding site (44). The overall structure of the active site is well conserved across a wide array of viruses and is commonly defined by a set of motifs (45). Of these, motifs A, B, and C form important interactions with the incoming NTP.

From available ternary structures of SARS-CoV-2, HCV, and FluB RdRp, primer/template and incoming NTP, we developed the models of how RDV-TP binds in its

## Broad-spectrum activity of remdesivir

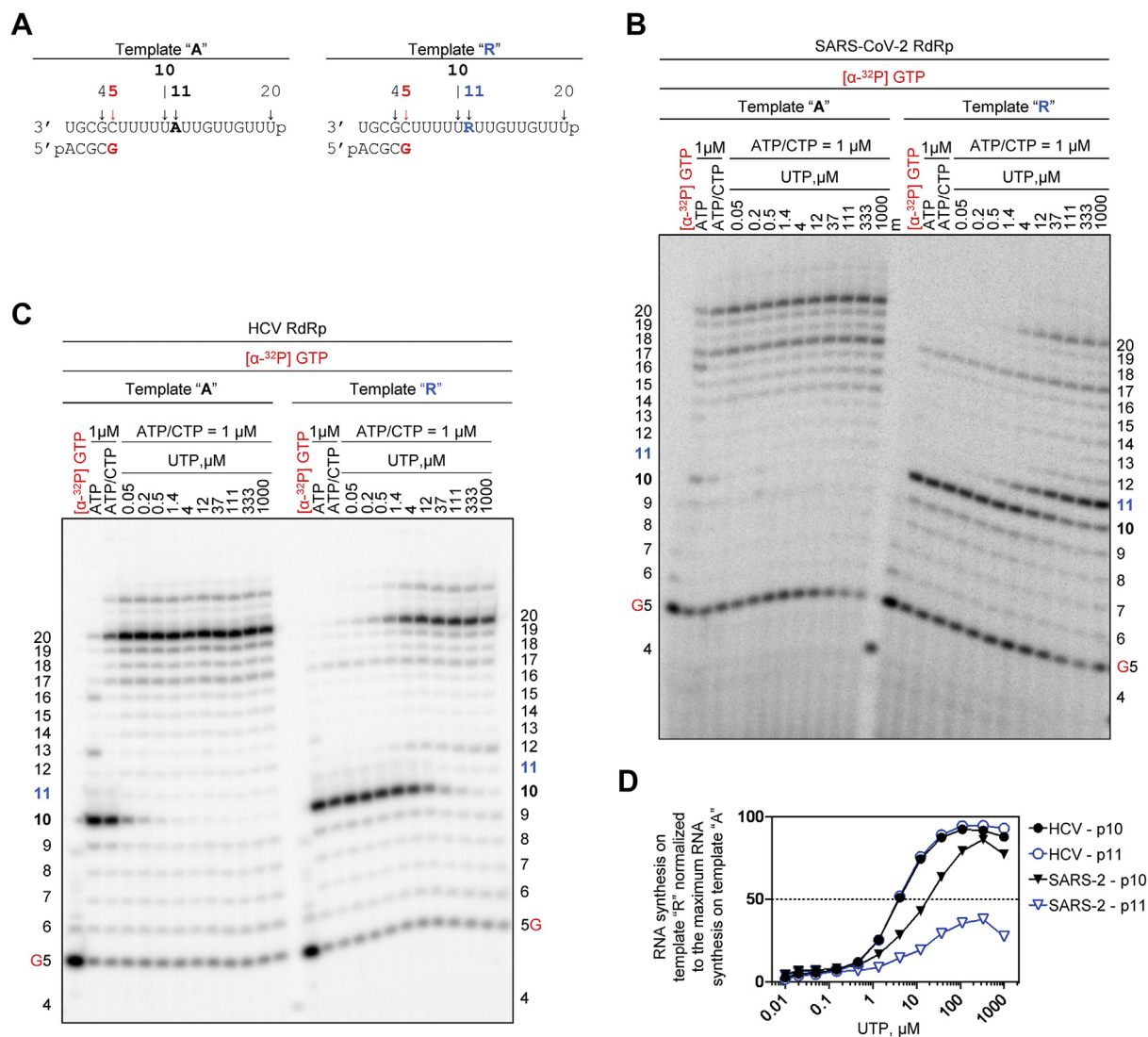


**Figure 3. Template-dependent inhibition of SARS-CoV-2 and HCV RdRp by an embedded RDV-MP.** A, RNA primer/template with an embedded AMP (Template "A", left) and RDV-MP (Template "R", right) at position 11. B, migration pattern of products of RNA synthesis catalyzed by SARS-CoV-2 RdRp, incorporation of ATP at position 12 is inhibited. C, reactions with HCV RdRp, incorporation of ATP at position 12 is not inhibited. D, graphical representation of RNA synthesis beyond position 10 and 11 (p10 and p11, respectively) on template "R". HCV, hepatitis C virus; MP, monophosphate; RdRp, RNA-dependent RNA polymerases; RDV, remdesivir; SARS-CoV-2, severe acute respiratory syndrome coronavirus 2.

preincorporated state as compared to ATP (Fig. 7). Consistent with our biochemical findings, SARS-CoV-2 and HCV RdRp enzymes show similar active sites for favorable binding of RDV-TP with virtually no distortion in position or alteration in how the ribose is recognized as compared to ATP. Moreover, the 1'-pocket is polar and therefore conducive to accommodating the 1'-cyano group of RDV-TP. In contrast, for FluB RdRp, polar residues at the active site appear to be too far to interact directly with the ribose portion of the NTP, as in SARS-CoV-2 and HCV. A WaterMap analysis predicted the presence of a water molecule in the nucleotide-binding site that facilitates recognition of the ribose 2'-OH (46, 47). However, the location of this water molecule overlaps with the location of the 1'-cyano group and would be necessarily displaced. A sequence alignment of FluB, LASV, and CCHFV enzymes suggests similarities, which may explain the poor incorporation of RDV-TP by these polymerases. Structures of

EBOV, NiV, and CCHFV RdRp enzymes are not available, and structures of RSV and LASV RdRp lack the RNA substrate, which is a limitation of our modeling approach.

Incorporation of a nucleotide analog at position "i" does not necessarily translate in inhibition of RNA synthesis. Structural evidence for inhibition at position "i + 3" has been provided for SARS-CoV-2 RdRp (27, 36, 39, 44). The conserved Ser-861 clashes with the 1'-cyano group of the incorporated RDV-MP and diminishes enzyme translocation. However, NTP concentrations >10  $\mu$ M are often sufficient to overcome the inhibition (26, 27, 36, 38, 39, 42). Interestingly, a very similar pattern is seen in the context of enterovirus A71 RdRp and may be ascribed to the equivalent Ser-417 (40). No significant inhibition was observed with HCV or dengue virus type 2 RdRp, both of which lack a structurally equivalent residue. Here, we have shown a subtle inhibitory effect at position "i" with HCV RdRp. RSV and EBOV RdRp show inhibition at

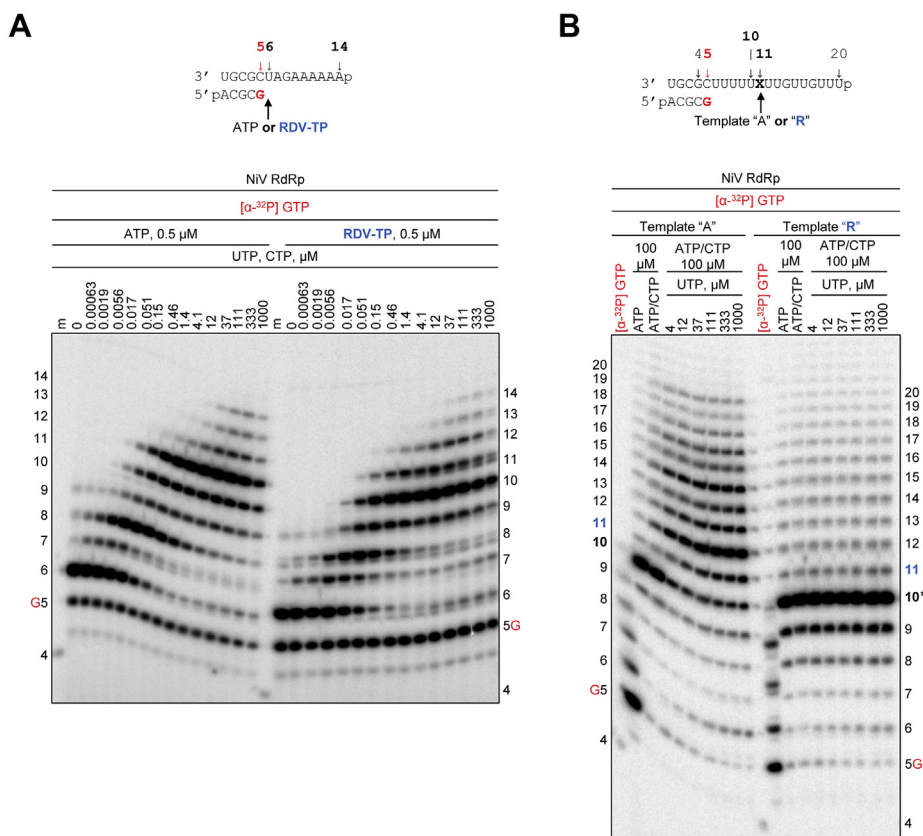


**Figure 4. RNA synthesis patterns following AMP and RDV-MP incorporation and template-dependent inhibition of NiV RdRp.** A, RNA primer/ template, as indicated in Figure 1 and migration pattern of products of RNA following the incorporation of AMP or RDV-MP. No inhibition is evident. B, RNA primer/ template, as indicated in Figure 3 and migration pattern of products of RNA synthesis opposite AMP (left) or RDV-MP (right). The asterisk at position 10 indicates the point of inhibition as a result of the embedded RDV-MP at position 11. MP, monophosphate; NiV, Nipah virus; RdRp, RNA-dependent RNA polymerases; RDV, remdesivir.

position  $i + 5$  (16); however, the structural reasons for these patterns remains elusive. Overall, this analysis suggests that the inhibitory effect in primer extension reactions is heterogeneous and generally weak. In contrast, the template-dependent inhibition of RNA synthesis seems to provide a uniform mechanism that shows strong inhibition of UTP incorporation opposite RDV-MP.

The template nucleotide that base pairs with the incoming nucleotide substrate is positioned through conserved interactions with the residues in motif F (Fig. 8). As seen in ternary structures of SARS-CoV-2, HCV, and FluB RdRp, the template base interacts with a bulky hydrophobic residue, whereas the ribose interacts with a second residue of varying character. These residues are separated by one additional residue, which is turned away from the template. In the case of SARS-CoV-2, the base moiety contacts V557, whereas the ribose interacts with G559. For HCV, similar interactions are seen with I160 and Y162, whereas for FluB, the equivalent interactions are with I241 and T243. A sequence alignment suggests that this submotif is conserved across all enzymes included in this study (Fig. 8). From the available structures, we have generated molecular models with the template incorporated RDV-MP positioned for UTP incorporation. In each case, the template RDV-MP 1'-cyano would be positioned between these two motif F residues, leading to a clash with the backbone

carbonyl of the middle residue. In SARS-CoV-2, the 1'-cyano is positioned too close to the carbonyl of A558 (42). Similarly, the 1'-cyano appears too close to the carbonyl of A242 in FluB as well. The hydrophobic nature of this area is likewise not conducive to placement of the polar cyano group and may also drive a shift in the position of template RDV. It is conceivable that this unfavorable environment is sufficient to prevent UTP binding or its proper alignment for incorporation. Although these details can vary across polymerases, a proposed uniform model is shown schematically in Figure 9. With fewer constraints on the single stranded 5' template overhang, RDV-MP is likely to be translocated to the active site without obstruction (Stages 1 and 2). The formation of a polymerase-competent complex with the incoming UTP is however constrained because of the putative steric problem between the 1'-cyano group of RDV-MP and motif F (Stage 3). Additional steric problems may also arise with the first translocation subsequent to UTP incorporation, but once past this point, further translocation does not appear to be impeded (Stage 4).

Taken together, the combined results of this biochemical study and previously reported cell-based data suggest a strong correlation between the antiviral effect of RDV, or its nucleoside parent, and effective use of RDV-TP as a substrate. The high selectivity of RDV-TP over ATP is a prerequisite for any downstream inhibitory effect. The patterns of inhibition of

## Broad-spectrum activity of remdesivir

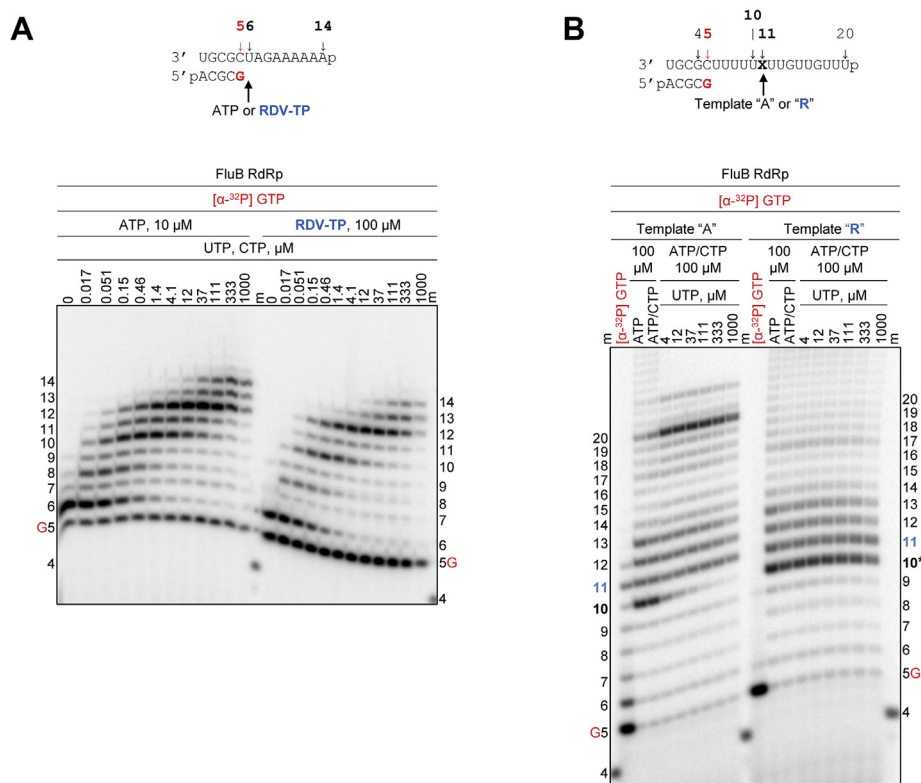


**Figure 5. RNA synthesis patterns following AMP and RDV-MP incorporation and template-dependent inhibition of FluB RdRp.** A, RNA primer/template, as indicated in Figure 1 and migration pattern of RNA products following the incorporation of AMP or RDV-MP. No inhibition is evident. B, RNA primer/template, as indicated in Figure 3 and migration pattern of RNA synthesis opposite AMP (left) or RDV-MP (right). The asterisk at position 10 indicates the point of inhibition as a result of the embedded RDV-MP at position 11. Flu B, influenza B; MP, monophosphate; RdRp, RNA-dependent RNA polymerase; RDV, remdesivir.

primer extension reactions can differ substantially depending on the nature of the polymerase. However, inhibition is usually inefficient at higher NTP concentrations. These are conditions that facilitate polymerase translocation and continuation of RNA synthesis. For coronaviruses, weak inhibition during synthesis of the first RNA strand might even be desired, so as to evade the intrinsic proofreading activity associated with the replication complex. A uniform mechanism of action is provided by the template-dependent inhibition of RNA synthesis opposite the embedded RDV-MP. The inhibition of incorporation of an incoming UTP base-pairing with RDV-MP is likely because of steric conflicts between the 1'-cyano group of RDV-MP and conserved residues of motif F. This inhibitory effect is seen with each of the diverse RdRp enzymes used in this study, including polymerases from the segmented negative-sense RNA viruses that are not sensitive to RDV. In these cases, the selective use of RDV-TP as substrate was poor. Thus, future drug development efforts that aim at a broader spectrum of antiviral activities should focus on improving the rates of incorporation while still capitalizing on the inhibitory effects of a bulky 1'-modification.

## Experimental procedures

### Nucleic acids and chemicals

RNA primers and templates used in this study were 5'-phosphorylated and purchased from Dharmacon. RDV-TP was provided by Gilead Sciences. NTPs were purchased

from GE Healthcare. [ $\alpha$ - $^{32}$ P]GTP was purchased from PerkinElmer.

### Protein expression and purification

Expression and purification of RNA-dependent RNA polymerases used in this study have been described (11, 25, 26, 42, 43, 48). We also used the baculovirus expression system for HCV nsp5b RdRp and NiV RdRp P/L complex. The pFastBac-1 (Invitrogen) plasmid with the codon-optimized synthetic DNA sequences (GenScript) coding for HCV nsp5b RdRp (CAB46677.1 polyprotein, residues 2420–3010) minus the 21 C-terminus residues was used as a starting material for protein expression in insect cells (Sf9, Invitrogen). We used the MultiBac (Geneva Biotech) system for protein expression in insect cells (Sf9, Invitrogen) according to the published protocols (49, 50). HCV nsp5b RdRp was purified using Ni-NTA affinity chromatography based on the C-terminal eight-histidine tag according to the manufacturer's specifications (Thermo Scientific). NiV RdRp P/L complex coding sequence (AEZ01385 and AEZ01390, P and L, respectively) was expressed in insect cells as a polyprotein in frame with N-terminal Tobacco etch virus protease. This approach was originally reported for the expression of influenza virus RdRp trimeric complex (51, 52). NiV P and L proteins were cleaved posttranslationally from the polyprotein at the engineered Tobacco etch virus sites. NiV RdRp P/L



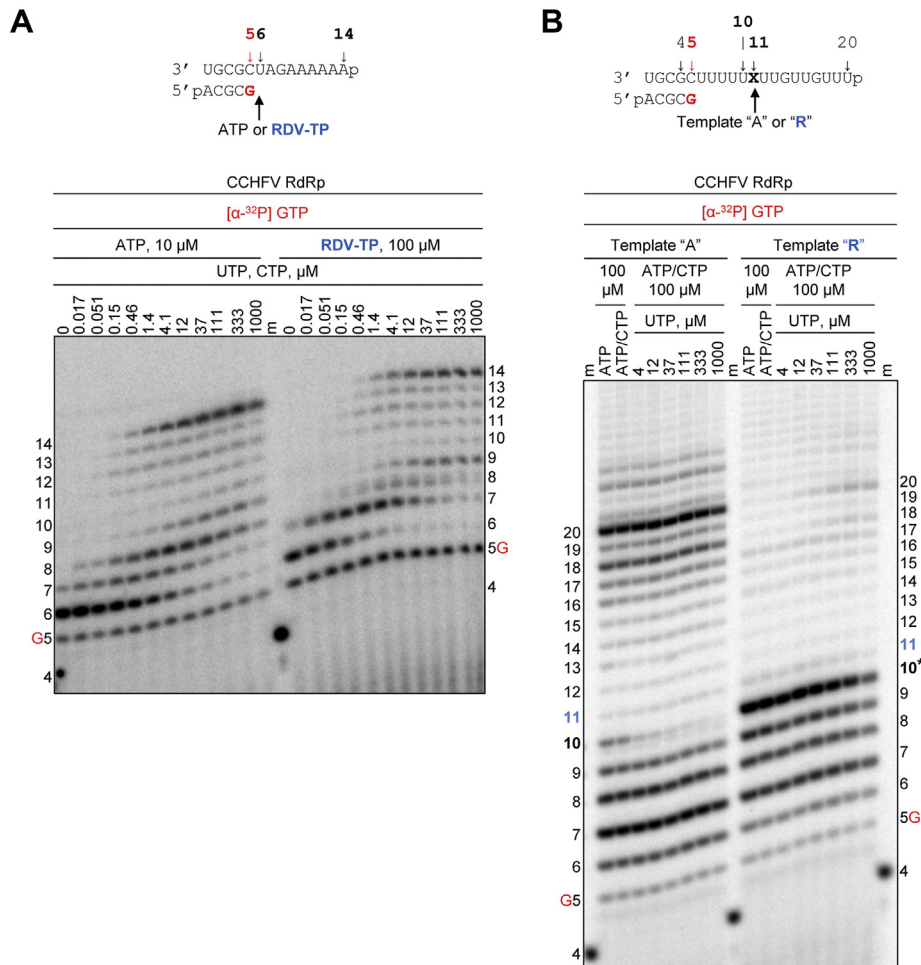


**Figure 6. RNA synthesis patterns following AMP and RDV-MP incorporation and template-dependent inhibition of CCHFV RdRp.** *A*, RNA primer/template, as indicated in Figure 1 and migration pattern of products of RNA following the incorporation of AMP or RDV-MP. No inhibition is evident. *B*, RNA primer/template, as indicated in Figure 3 and migration pattern of RNA synthesis opposite AMP (left) or RDV-MP (right). The asterisk at position 10 indicates the point of inhibition as a result of the embedded RDV-MP at position 11. CCHFV, Crimean-Congo hemorrhagic fever virus; MP, monophosphate; RdRp, RNA-dependent RNA polymerases; RDV, remdesivir.

complex was purified using Ni-NTA affinity chromatography based on the P protein N-terminal eight-histidine tag according to the manufacturer’s specifications (Thermo Scientific). The protein identities of the purified HCV nsp5b RdRp and NiV RdRp P/L complex were confirmed by mass spectrometry analysis (Alberta Proteomics and Mass Spectrometry).

**Evaluation of nucleotide incorporation and the effect of primer- or template-embedded remdesivir on viral RNA synthesis**

The following synthetic 5'-monophosphorylated RNA templates were used in this study (the portion of the template which is complementary to the 4-nt primer is underlined): 3'UGCGCUAGAAAAA p for measurements of the RDV-TP selectivity values and determination of the patterns of inhibition of RNA synthesis subsequent to an incorporated RDV at single position; 3'UGCGCUAGUUUUUUUUUUUUUUUUU p for ATP/RDV-TP competition experiments; 3'UGCGCUUUUURUUGUUGUUU p for the evaluation of nucleotide

incorporation opposite template-embedded remdesivir (R, template “R”) in comparison to templated adenosine at the equivalent position (template “A”). Both RNA templates were produced in the lab as previously described by us (42). RNA synthesis assays of viral RdRp, data acquisition, and quantification were performed as previously reported by us (16, 25, 26, 42, 43). Briefly, the concentrations of various viral RdRp proteins and protein complexes were selected such that incorporation of [ $\alpha$ -<sup>32</sup>P]-GTP was linear during single nucleotide incorporation studies. The ranges of ATP and RDV-TP concentrations used to determine the selectivity values were optimized such that minimal misincorporations at subsequent positions were observed. In reactions involving primer- or template-embedded remdesivir, the viral enzyme concentrations were optimized to promote full template-length RNA synthesis. Standard reaction mixture for RNA synthesis assays (final concentrations after mixing) included optimal concentrations of the purified viral RdRp, Tris–HCl (pH 8, 25 mM), RNA primer (200 μM), RNA template (2 μM, except for FluB RdRp reactions where optimal RNA template concentration was 0.5 μM), [ $\alpha$ -<sup>32</sup>P]-GTP (0.1 μM), and various

## Broad-spectrum activity of remdesivir

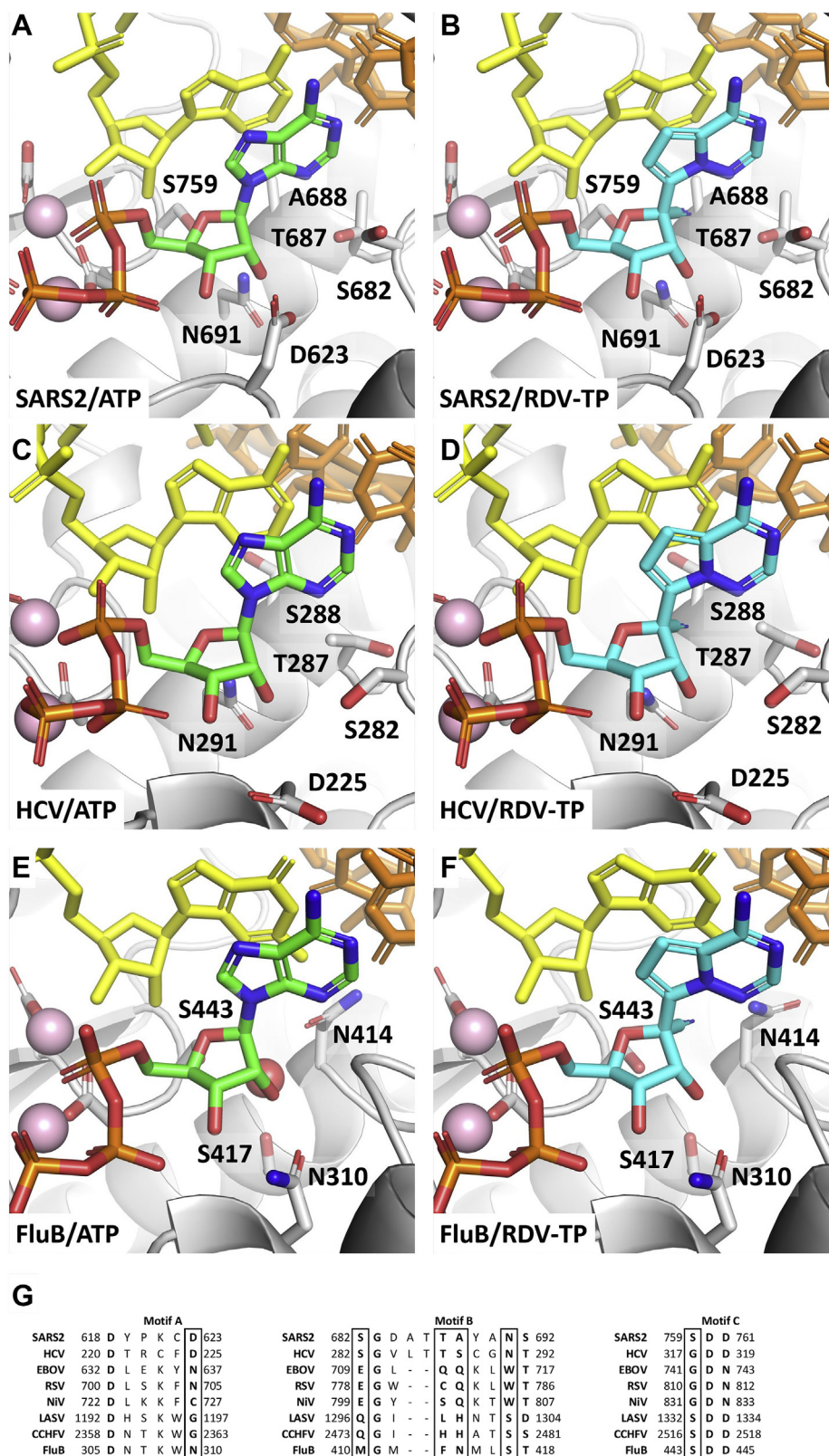


**Figure 7. Models of the active site of viral RdRp enzymes.** Models of ATP and RDV-TP in their preincorporation states for SARS-CoV-2 (A and B), HCV (C and D), and FluB (E and F) RdRps. RDV-TP is seen to be a good substrate for SARS-CoV-2 and HCV, showing little difference in binding position relative to ATP. However, RDV-TP displaces a water molecule critical to recognition of the ribose 2'OH in FluB, compromising its binding affinity. G, a comparison of the key motifs that make up the polymerase active site suggests that LASV and CCHFV may recognize the NTP in a manner more similar to FluB, whereas EBOV and RSV likely recognize the NTP by a different set of interactions. CCHFV, Crimean-Congo hemorrhagic fever virus; EBOV, Zaire Ebola virus; Flu B, influenza B; HCV, hepatitis C virus; LASV, Lassa virus; RdRp, RNA-dependent RNA polymerases; RDV, remdesivir; RSV, respiratory syncytial virus; SARS-CoV-2, severe acute respiratory syndrome coronavirus 2; TP, triphosphate.

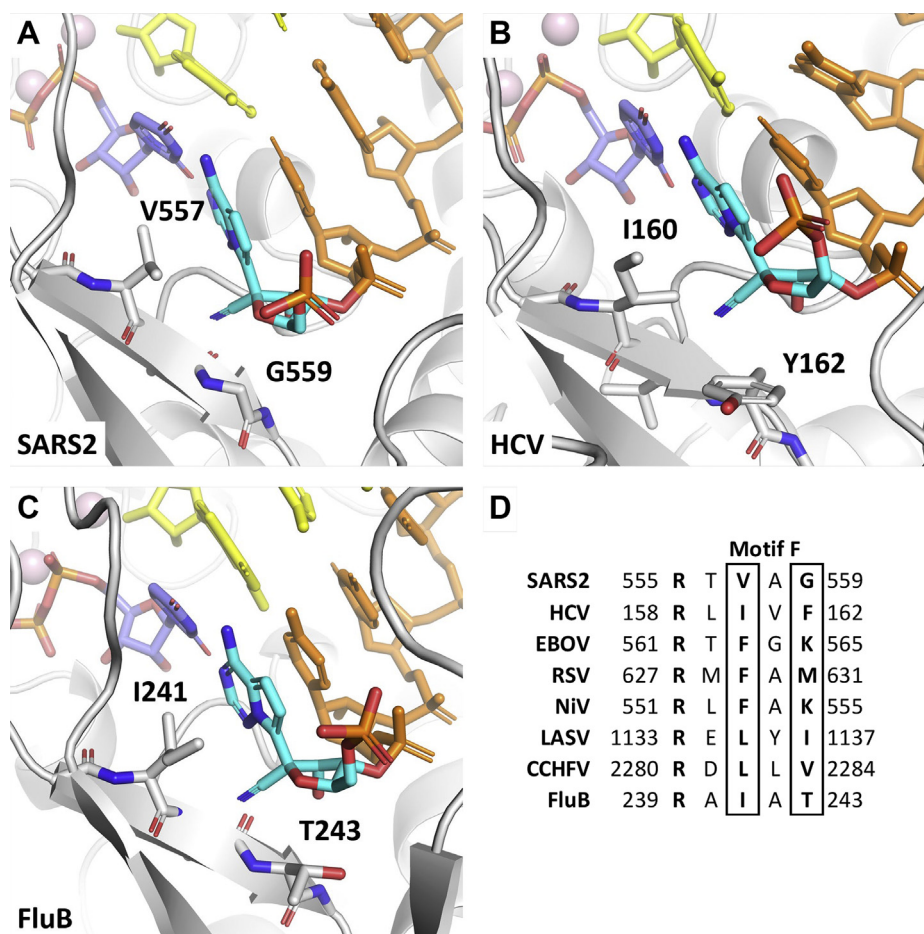


**Figure 8. Models of conserved residues of motif F.** Template-dependent inhibition by RDV is shown here for (A) SARS-CoV-2, (B) HCV, and (C) FluB RdRps. The 1'-CN of template incorporated RDV-MP is positioned between two typically hydrophobic residues, pushing against the backbone of the intermediate residue. D, as the overall structure of Motif F is widely conserved, if not the exact sequence, this represents a uniform mechanism of inhibition across a diverse set of polymerases. Flu B, influenza B; HCV, hepatitis C virus; MP, monophosphate; RdRp, RNA-dependent RNA polymerases; RDV, remdesivir; SARS-CoV-2, severe acute respiratory syndrome coronavirus 2.

concentrations and combinations (as indicated) of NTP and RDV-TP. Partial (minus  $\text{MgCl}_2$ ) reaction mixtures (10  $\mu\text{l}$ ) were prepared on ice and incubated for 5 to 10 min at 30 °C followed by the addition of 5  $\mu\text{l}$  of  $\text{MgCl}_2$  (5 mM) to initiate nucleotide incorporation. The reactions were stopped after 30 min by the addition of 15  $\mu\text{l}$  of formamide/EDTA (50 mM) mixture and incubated at 95 °C for 10 min. The reaction products were resolved through 20% PAGE, and the  $[\alpha\text{-}^{32}\text{P}]$ -generated signal was stored and scanned from phosphor-imager screens. The data were analyzed using GraphPad Prism 7.0 (GraphPad Software, Inc).

### Molecular modeling

To date, a well resolved preincorporation state for SARS-CoV-2, in which the NTP is positioned in the active site with suitable primer and template RNA, has not been determined by cryo-EM. A model of the preincorporation state of RDV-TP in SARS-CoV-2 has previously been described (26, 42). Based on more recent cryo-EM structures, including PDB:6XEZ (53), which captures the SARS-CoV-2 polymerase complex ( $\text{nsp12/nsp7}/(\text{nsp8})_2/(\text{nsp13})_2$ ) with primer and template RNA bound, the model has since been updated using similar approaches to those outlined previously. The models

for HCV were based on the x-ray structures PDB:4WTA and PDB:4WTD (54), which capture preincorporation states of UDP and ADP, respectively. The models for FluB were based on the cryo-EM structures PDB:6QCV and PDB:6QCT (55), which capture the preincorporation initiation state and the elongation state, respectively. All optimization was performed with Macromodel and Prime in the Schrödinger Suite (56, 57). The identification of a water molecule in the active site of FluB, which establishes a hydrogen bond network between the protein and the NTP, was carried out with WaterMap, also part of the Schrödinger Suite (46, 47).

### Data availability

All data are included within this article

*Supporting information*—This article contains supporting information.

*Acknowledgments*—The authors would like to thank Emma Woolner and Dana Kocincova for excellent technical assistance and Dr Jack Moore at the Alberta Proteomics and Mass Spectrometry facility for mass spectrometry analysis.

## Broad-spectrum activity of remdesivir

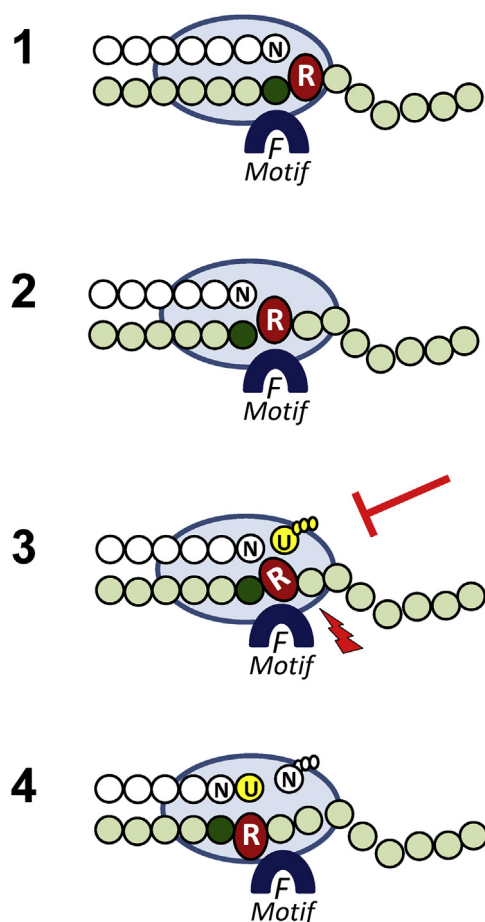


**Figure 9. A uniform model of the mechanism of action of RDV.** Stage 1, the priming strand is shown with white circles, green circles represent residues of the template, the light blue oval represents RdRp, the dark blue semi-circle represents motif F, the red oval (R) represents RDV-MP with its 1'-cyano group, and the dark green circle represents the templating nucleotide that precedes RDV-MP. The complex is here shown immediately after nucleotide (N) incorporation. Stages 2 and 3, molecular modeling predicts a steric clash between the 1'-cyano group and motif F. The magnitude of the clash (red arrow) is a function of the sequence variation in motif F across the various viral RdRp and will determine the extent of UTP (yellow) incorporation. For HCV and SARS-CoV-2 RdRp, higher UTP concentrations can overcome inhibition. For SARS-CoV-2 RdRp, another obstacle arises at the level of the subsequent nucleotide incorporation (white) that is observed in our biochemical assays (Stage 4). HCV, hepatitis C virus; MP, monophosphate; RdRp, RNA-dependent RNA polymerases; RDV, remdesivir; SARS-CoV-2, severe acute respiratory syndrome coronavirus 2.

**Author contributions**—C. J. G., H. W. L., E. P. T., and J. K. P. investigation; C. J. G. and H. W. L. validation; C. J. G., H. W. L., E. P. T., J. K. P., and M. G. formal analysis; C. J. G., H. W. L., E. P. T., and J. K. P. visualization; C. J. G., H. W. L., E. P. T., and M. G. writing—original draft; J. K. P., J. Y. F., J. P. B., D. P. P., and M. G. writing—review and editing; J. Y. F., J. P. B., and D. P. P. resources; M. G. conceptualization; M. G. methodology; M. G. supervision; M. G. funding acquisition.

**Funding and additional information**—This study was supported by grants to M. G. from the Canadian Institutes of Health Research (CIHR, grant number 170343) and from the Alberta Ministry of Jobs, Economy and Innovation by the Major Innovation Fund Program for the AMR – One Health Consortium. M. G. received funding from Gilead Sciences in support for studies on the mechanism of action of remdesivir. J. K. P., J. Y. F., J. P. B., and D. P. P. are Gilead employees.

**Conflict of interest**—The authors declare that they have no conflicts of interest with the contents of this article.

**Abbreviations**—The abbreviations used are: CCHFV, Crimean-Congo hemorrhagic fever virus; COVID-19, coronavirus disease 2019; EBOV, Zaire Ebola virus; Flu B, influenza B; HCV, hepatitis C virus; LASV, Lassa virus; MERS-CoV, Middle Eastern respiratory syndrome; MP, monophosphate; NiV, Nipah virus; RdRp, RNA-dependent RNA polymerases; RDV, remdesivir; RSV, respiratory syncytial virus; SARS-CoV-2, severe acute respiratory syndrome coronavirus 2; TP, triphosphate.

## References

- Lu, R., Zhao, X., Li, J., Niu, P., Yang, B., Wu, H., Wang, W., Song, H., Huang, B., Zhu, N., Bi, Y., Ma, X., Zhan, F., Wang, L., Hu, T., *et al.* (2020) Genomic characterisation and epidemiology of 2019 novel coronavirus: Implications for virus origins and receptor binding. *Lancet* **395**, 565–574
- Zhu, N., Zhang, D., Wang, W., Li, X., Yang, B., Song, J., Zhao, X., Huang, B., Shi, W., Lu, R., Niu, P., Zhan, F., Ma, X., Wang, D., Xu, W., *et al.* (2020) A novel coronavirus from patients with pneumonia in China, 2019. *N. Engl. J. Med.* **382**, 727–733
- Baden, L. R., El Sahly, H. M., Essink, B., Kotloff, K., Frey, S., Novak, R., Diemert, D., Spector, S. A., Rouphael, N., Creech, C. B., McGettigan, J., Khetan, S., Segall, N., Solis, J., Brosz, A., *et al.* (2021) Efficacy and safety of the mRNA-1273 SARS-CoV-2 vaccine. *N. Engl. J. Med.* **384**, 403–416
- Polack, F. P., Thomas, S. J., Kitchin, N., Absalon, J., Gurtman, A., Lockhart, S., Perez, J. L., Perez Marc, G., Moreira, E. D., Zerbini, C., Bailey, R., Swanson, K. A., Roychoudhury, S., Koury, K., Li, P., *et al.* (2020) Safety and efficacy of the BNT162b2 mRNA Covid-19 vaccine. *N. Engl. J. Med.* **383**, 2603–2615
- Voysey, M., Clemens, S. A. C., Madhi, S. A., Weckx, L. Y., Folegatti, P. M., Aley, P. K., Angus, B., Baillie, V. L., Barnabas, S. L., Bhorat, Q. E., Bibi, S., Briner, C., Cicconi, P., Collins, A. M., Colin-Jones, R., *et al.* (2021) Safety and efficacy of the ChAdOx1 nCoV-19 vaccine (AZD1222) against SARS-CoV-2: An interim analysis of four randomised controlled trials in Brazil, South Africa, and the UK. *Lancet* **397**, 99–111
- Sadoff, J., Le Gars, M., Shukarev, G., Heerwegh, D., Truyers, C., de Groot, A. M., Stoop, J., Tete, S., Van Damme, W., Leroux-Roels, I., Berghmans, P. J., Kimmel, M., Van Damme, P., de Hoon, J., Smith, W., *et al.* (2021) Interim results of a phase 1-2a trial of Ad26.COV2.S Covid-19 vaccine. *N. Engl. J. Med.* **384**, 1824–1835
- US Food and Drug Administration. (2020) *Fact Sheet for Health Care Providers. Emergency Use Authorization (EUA) of Veklury (Remdesivir)*. Food and Drug Administration, Silver Spring, MD: 1–20
- Agostini, M. L., Andres, E. L., Sims, A. C., Graham, R. L., Sheahan, T. P., Lu, X., Smith, E. C., Case, J. B., Feng, J. Y., Jordan, R., Ray, A. S., Cihlar, T., Siegel, D., Mackman, R. L., Clarke, M. O., *et al.* (2018) Coronavirus susceptibility to the antiviral remdesivir (GS-5734) is mediated by the viral polymerase and the proofreading exoribonuclease. *mBio* **9**, e00221-18
- Brown, A. J., Won, J. J., Graham, R. L., Dinnon, K. H., 3rd, Sims, A. C., Feng, J. Y., Cihlar, T., Denison, M. R., Baric, R. S., and Sheahan, T. P. (2019) Broad spectrum antiviral remdesivir inhibits human endemic and zoonotic deltacoronaviruses with a highly divergent RNA dependent RNA polymerase. *Antiviral Res.* **169**, 104541
- de Wit, E., Feldmann, F., Cronin, J., Jordan, R., Okumura, A., Thomas, T., Scott, D., Cihlar, T., and Feldmann, H. (2020) Prophylactic and therapeutic remdesivir (GS-5734) treatment in the rhesus macaque model of MERS-CoV infection. *Proc. Natl. Acad. Sci. U. S. A.* **117**, 6771–6776
- Jordan, P. C., Liu, C., Raynaud, P., Lo, M. K., Spiropoulou, C. F., Symons, J. A., Beigelman, L., and Deval, J. (2018) Initiation, extension, and termination of RNA synthesis by a paramyxovirus polymerase. *PLoS Pathog.* **14**, e1006889
- Lo, M. K., Feldmann, F., Gary, J. M., Jordan, R., Bannister, R., Cronin, J., Patel, N. R., Klena, J. D., Nichol, S. T., Cihlar, T., Zaki, S. R., Feldmann, H., Spiropoulou, C. F., and de Wit, E. (2019) Remdesivir (GS-5734) protects African green monkeys from Nipah virus challenge. *Sci. Transl. Med.* **11**, eaau9242

13. Lo, M. K., Jordan, R., Arvey, A., Sudhamsu, J., Shrivastava-Ranjan, P., Hotard, A. L., Flint, M., McMullan, L. K., Siegel, D., Clarke, M. O., Mackman, R. L., Hui, H. C., Perron, M., Ray, A. S., Cihlar, T., *et al.* (2017) GS-5734 and its parent nucleoside analog inhibit Filo-, Pneumo-, and Paramyxoviruses. *Sci. Rep.* **7**, 43395
14. Sheahan, T. P., Sims, A. C., Graham, R. L., Menachery, V. D., Gralinski, L. E., Case, J. B., Leist, S. R., Pycr, K., Feng, J. Y., Trantcheva, I., Bannister, R., Park, Y., Babusis, D., Clarke, M. O., Mackman, R. L., *et al.* (2017) Broad-spectrum antiviral GS-5734 inhibits both epidemic and zoonotic coronaviruses. *Sci. Transl. Med.* **9**, eaal3653
15. Sheahan, T. P., Sims, A. C., Leist, S. R., Schafer, A., Won, J., Brown, A. J., Montgomery, S. A., Hogg, A., Babusis, D., Clarke, M. O., Spahn, J. E., Bauer, L., Sellers, S., Porter, D., Feng, J. Y., *et al.* (2020) Comparative therapeutic efficacy of remdesivir and combination lopinavir, ritonavir, and interferon beta against MERS-CoV. *Nat. Commun.* **11**, 222
16. Tchesnokov, E. P., Feng, J. Y., Porter, D. P., and Gotte, M. (2019) Mechanism of inhibition of Ebola virus RNA-dependent RNA polymerase by remdesivir. *Viruses* **11**, 326
17. Warren, T. K., Jordan, R., Lo, M. K., Ray, A. S., Mackman, R. L., Soloveva, V., Siegel, D., Perron, M., Bannister, R., Hui, H. C., Larson, N., Strickley, R., Wells, J., Stuthman, K. S., Van Tongeren, S. A., *et al.* (2016) Therapeutic efficacy of the small molecule GS-5734 against Ebola virus in rhesus monkeys. *Nature* **531**, 381–385
18. Siegel, D., Hui, H. C., Doerffler, E., Clarke, M. O., Chun, K., Zhang, L., Neville, S., Carra, E., Lew, W., Ross, B., Wang, Q., Wolfe, L., Jordan, R., Soloveva, V., Knox, J., *et al.* (2017) Discovery and synthesis of a phosphoramidate prodrug of a pyrrolo[2,1-f][triazin-4-amino] adenine C-nucleoside (GS-5734) for the treatment of Ebola and emerging viruses. *J. Med. Chem.* **60**, 1648–1661
19. Puijssers, A. J., George, A. S., Schafer, A., Leist, S. R., Gralinski, L. E., Dinnon, K. H., 3rd, Yount, B. L., Agostini, M. L., Stevens, L. J., Chappell, J. D., Lu, X., Hughes, T. M., Gully, K., Martinez, D. R., Brown, A. J., *et al.* (2020) Remdesivir inhibits SARS-CoV-2 in human lung cells and chimeric SARS-CoV expressing the SARS-CoV-2 RNA polymerase in mice. *Cell Rep.* **32**, 107940
20. Cho, A., Saunders, O. L., Butler, T., Zhang, L., Xu, J., Vela, J. E., Feng, J. Y., Ray, A. S., and Kim, C. U. (2012) Synthesis and antiviral activity of a series of 1'-substituted 4-aza-7,9-dideazaadenosine C-nucleosides. *Bioorg. Med. Chem. Lett.* **22**, 2705–2707
21. Mulangu, S., Dodd, L. E., Davey, R. T., Jr., Tshiani Mbaya, O., Proschan, M., Mukadi, D., Lusakibanza Manzo, M., Nzolo, D., Tshomba Oloma, A., Ibanda, A., Ali, R., Coulibaly, S., Levine, A. C., Grais, R., Diaz, J., *et al.* (2019) A randomized, controlled trial of Ebola virus disease therapeutics. *N. Engl. J. Med.* **381**, 2293–2303
22. Grein, J., Ohmagari, N., Shin, D., Diaz, G., Asperges, E., Castagna, A., Feldt, T., Green, G., Green, M. L., Lescure, F.-X., Nicastri, E., Oda, R., Yo, K., Quiros-Roldan, E., Studemeister, A., *et al.* (2020) Compassionate use of remdesivir for patients with severe Covid-19. *N. Engl. J. Med.* **382**, 2327–2336
23. Beigel, J. H., Tomashek, K. M., Dodd, L. E., Mehta, A. K., Zingman, B. S., Kalil, A. C., Hohmann, E., Chu, H. Y., Luetkemeyer, A., Kline, S., Lopez de Castilla, D., Finberg, R. W., Dierberg, K., Tapson, V., Hsieh, L., *et al.* (2020) Remdesivir for the treatment of Covid-19 - final report. *N. Engl. J. Med.* **383**, 1813–1826
24. WHO Solidarity Trial Consortium, Pan, H., Peto, R., Henao-Restrepo, A. M., Preziosi, M. P., Sathiyamoorthy, V., Abdool Karim, Q., Alejandria, M. M., Hernández García, C., Kieny, M. P., Malekzadeh, R., Murthy, S., Reddy, K. S., Roses Periago, M., Abi Hanna P, *et al.* (2021) Repurposed antiviral drugs for Covid-19—interim WHO solidarity trial results. *N. Engl. J. Med.* **384**, 497–511
25. Gordon, C. J., Tchesnokov, E. P., Feng, J. Y., Porter, D. P., and Gotte, M. (2020) The antiviral compound remdesivir potently inhibits RNA-dependent RNA polymerase from Middle East respiratory syndrome coronavirus. *J. Biol. Chem.* **295**, 4773–4779
26. Gordon, C. J., Tchesnokov, E. P., Woolner, E., Perry, J. K., Feng, J. Y., Porter, D. P., and Gotte, M. (2020) Remdesivir is a direct-acting antiviral that inhibits RNA-dependent RNA polymerase from severe acute respiratory syndrome coronavirus 2 with high potency. *J. Biol. Chem.* **295**, 6785–6797
27. Wang, Q., Wu, J., Wang, H., Gao, Y., Liu, Q., Mu, A., Ji, W., Yan, L., Zhu, Y., Zhu, C., Fang, X., Yang, X., Huang, Y., Gao, H., Liu, F., *et al.* (2020) Structural basis for RNA replication by the SARS-CoV-2 polymerase. *Cell* **182**, 417–428.e13
28. Dangerfield, T. L., Huang, N. Z., and Johnson, K. A. (2020) Remdesivir is effective in combating COVID-19 because it is a better substrate than ATP for the viral RNA-dependent RNA polymerase. *iScience* **23**, 101849
29. Boyer, P. L., Julias, J. G., Marquez, V. E., and Hughes, S. H. (2005) Fixed conformation nucleoside analogs effectively inhibit excision-proficient HIV-1 reverse transcriptases. *J. Mol. Biol.* **345**, 441–450
30. Boyer, P. L., Julias, J. G., Ambrose, Z., Siddiqui, M. A., Marquez, V. E., and Hughes, S. H. (2007) The nucleoside analogs 4'C-methyl thymidine and 4'C-ethyl thymidine block DNA synthesis by wild-type HIV-1 RT and excision proficient NRTI resistant RT variants. *J. Mol. Biol.* **371**, 873–882
31. Langley, D. R., Walsh, A. W., Baldick, C. J., Eggers, B. J., Rose, R. E., Levine, S. M., Kapur, A. J., Colonna, R. J., and Tenney, D. J. (2007) Inhibition of hepatitis B virus polymerase by entecavir. *J. Virol.* **81**, 3992–4001
32. Tchesnokov, E. P., Obikhod, A., Schinazi, R. F., and Gotte, M. (2008) Delayed chain termination protects the anti-hepatitis B virus drug entecavir from excision by HIV-1 reverse transcriptase. *J. Biol. Chem.* **283**, 34218–34228
33. Deval, J. (2009) Antimicrobial strategies: Inhibition of viral polymerases by 3'-hydroxyl nucleosides. *Drugs* **69**, 151–166
34. Michailidis, E., Huber, A. D., Ryan, E. M., Ong, Y. T., Leslie, M. D., Matzek, K. B., Singh, K., Marchand, B., Hagedorn, A. N., Kirby, K. A., Rohan, L. C., Kodama, E. N., Mitsuya, H., Parniak, M. A., and Sarafianos, S. G. (2014) 4'-Ethynyl-2-fluoro-2'-deoxyadenosine (EFdA) inhibits HIV-1 reverse transcriptase with multiple mechanisms. *J. Biol. Chem.* **289**, 24533–24548
35. Chen, H., Lawler, J. L., Filman, D. J., Hogle, J. M., and Coen, D. M. (2021) Resistance to a nucleoside analog antiviral drug from more rapid extension of drug-containing primers. *mBio* **12**, e03492-20
36. Kocic, G., Hillen, H. S., Tegunov, D., Dienemann, C., Seitz, F., Schmitzova, J., Farnung, L., Siewert, A., Hobartner, C., and Cramer, P. (2021) Mechanism of SARS-CoV-2 polymerase stalling by remdesivir. *Nat. Commun.* **12**, 279
37. Seifert, M., Bera, S. C., van Nies, P., Kirchdoerfer, R. N., Shannon, A., Le, T. T., Meng, X., Xia, H., Wood, J. M., Harris, L. D., Papini, F. S., Arnold, J. J., Almo, S., Grove, T. L., Shi, P. Y., *et al.* (2021) Inhibition of SARS-CoV-2 polymerase by nucleotide analogs from a single-molecule perspective. *Elife* **10**, e70968
38. Lu, G., Zhang, X., Zheng, W., Sun, J., Hua, L., Xu, L., Chu, X. J., Ding, S., and Xiong, W. (2020) Development of a simple in vitro assay to identify and evaluate nucleotide analogs against SARS-CoV-2 RNA-dependent RNA polymerase. *Antimicrob. Agents Chemother.* **65**, e01508-20
39. Bravo, J. P. K., Dangerfield, T. L., Taylor, D. W., and Johnson, K. A. (2021) Remdesivir is a delayed translocation inhibitor of SARS-CoV-2 replication. *Mol. Cell* **81**, 1548–1552.e4
40. Wu, J., Wang, H., Liu, Q., Li, R., Gao, Y., Fang, X., Zhong, Y., Wang, M., Wang, Q., Rao, Z., and Gong, P. (2021) Remdesivir overcomes the S861 roadblock in SARS-CoV-2 polymerase elongation complex. *Cell Rep.* **37**, 109882
41. Wang, J., Reiss, K., Shi, Y., Lolis, E., Lisi, G. P., and Batista, V. S. (2021) Mechanism of inhibition of the reproduction of SARS-CoV-2 and Ebola viruses by remdesivir. *Biochemistry* **60**, 1869–1875
42. Tchesnokov, E. P., Gordon, C. J., Woolner, E., Kocinkova, D., Perry, J. K., Feng, J. Y., Porter, D. P., and Gotte, M. (2020) Template-dependent inhibition of coronavirus RNA-dependent RNA polymerase by remdesivir reveals a second mechanism of action. *J. Biol. Chem.* **295**, 16156–16165
43. Tchesnokov, E. P., Bailey-Elkin, B. A., Mark, B. L., and Gotte, M. (2020) Independent inhibition of the polymerase and deubiquitinase activities of the Crimean-Congo hemorrhagic fever virus full-length L-protein. *PLoS Negl. Trop. Dis.* **14**, e0008283
44. Yin, W., Mao, C., Luan, X., Shen, D. D., Shen, Q., Su, H., Wang, X., Zhou, F., Zhao, W., Gao, M., Chang, S., Xie, Y. C., Tian, G., Jiang, H. W., Tao, S. C., *et al.* (2020) Structural basis for inhibition of the RNA-dependent RNA polymerase from SARS-CoV-2 by remdesivir. *Science* **368**, 1499–1504

## Broad-spectrum activity of remdesivir

45. te Velthuis, A. J. (2014) Common and unique features of viral RNA-dependent polymerases. *Cell. Mol. Life Sci.* **71**, 4403–4420
46. Young, T., Abel, R., Kim, B., Berne, B. J., and Friesner, R. A. (2007) Motifs for molecular recognition exploiting hydrophobic enclosure in protein-ligand binding. *Proc. Natl. Acad. Sci. U. S. A.* **104**, 808–813
47. Abel, R., Young, T., Farid, R., Berne, B. J., and Friesner, R. A. (2008) Role of the active-site solvent in the thermodynamics of factor Xa ligand binding. *J. Am. Chem. Soc.* **130**, 2817–2831
48. Tchesnokov, E. P., Raesisimakiani, P., Ngure, M., Marchant, D., and Gotte, M. (2018) Recombinant RNA-dependent RNA polymerase complex of Ebola virus. *Sci. Rep.* **8**, 3970
49. Berger, I., Fitzgerald, D. J., and Richmond, T. J. (2004) Baculovirus expression system for heterologous multiprotein complexes. *Nat. Biotechnol.* **22**, 1583–1587
50. Bieniossek, C., Richmond, T. J., and Berger, I. (2008) MultiBac: Multigene baculovirus-based eukaryotic protein complex production. *Curr. Protoc. Protein Sci.* Chapter 5:Unit 5.20
51. Pflug, A., Guilligay, D., Reich, S., and Cusack, S. (2014) Structure of influenza A polymerase bound to the viral RNA promoter. *Nature* **516**, 355–360
52. Reich, S., Guilligay, D., Pflug, A., Malet, H., Berger, I., Crepin, T., Hart, D., Lunardi, T., Nanao, M., Ruigrok, R. W., and Cusack, S. (2014) Structural insight into cap-snatching and RNA synthesis by influenza polymerase. *Nature* **516**, 361–366
53. Chen, J., Malone, B., Llewellyn, E., Grasso, M., Shelton, P. M. M., Olinares, P. D. B., Maruthi, K., Eng, E. T., Vatandaslar, H., Chait, B. T., Kapoor, T. M., Darst, S. A., and Campbell, E. A. (2020) Structural basis for helicase-polymerase coupling in the SARS-CoV-2 replication-transcription complex. *Cell* **182**, 1560–1573.e13
54. Appleby, T. C., Perry, J. K., Murakami, E., Barauskas, O., Feng, J., Cho, A., Fox, D., 3rd, Wetmore, D. R., McGrath, M. E., Ray, A. S., Sofia, M. J., Swaminathan, S., and Edwards, T. E. (2015) Viral replication. Structural basis for RNA replication by the hepatitis C virus polymerase. *Science* **347**, 771–775
55. Kouba, T., Drncova, P., and Cusack, S. (2019) Structural snapshots of actively transcribing influenza polymerase. *Nat. Struct. Mol. Biol.* **26**, 460–470
56. Jacobson, M. P., Pincus, D. L., Rapp, C. S., Day, T. J., Honig, B., Shaw, D. E., and Friesner, R. A. (2004) A hierarchical approach to all-atom protein loop prediction. *Proteins* **55**, 351–367
57. Jacobson, M. P., Friesner, R. A., Xiang, Z., and Honig, B. (2002) On the role of the crystal environment in determining protein side-chain conformations. *J. Mol. Biol.* **320**, 597–608
58. Xie, X., Muruato, A. E., Zhang, X., Lokugamage, K. G., Fontes-Garfias, C. R., Zou, J., Liu, J., Ren, P., Balakrishnan, M., Cihlar, T., Tseng, C. K., Makino, S., Menachery, V. D., Bilello, J. P., and Shi, P. Y. (2020) A nanoluciferase SARS-CoV-2 for rapid neutralization testing and screening of anti-infective drugs for COVID-19. *Nat. Commun.* **11**, 5214